JOURNAL OF GEOPHYSICAL RESEARCH, VOL. 115, A06207, doi:10.1029/2009JA014262, 2010

A new form of Saturn's magnetopause using a dynamic pressure balance model, based on in situ, multi-instrument Cassini measurements

S. J. Kanani,[1,2] C. S. Arridge,[1,2] G. H. Jones,[1,2] A. N. Fazakerley,[1] H. J. McAndrews,[3] N. Sergis,[4] S. M. Krimigis,[5] M. K. Dougherty,[6] A. J. Coates,[1,2] D. T. Young,[7] K. C. Hansen,[8] and N. Krupp[9]

Received 17 March 2009; revised 3 November 2009; accepted 4 January 2010; published 17 June 2010.

[1] The shape and location of a planetary magnetopause can be determined by balancing the solar wind dynamic pressure with the magnetic and thermal pressures found inside the boundary. Previous studies have found the kronian magnetosphere to show rigidity (like that of Earth) as well as compressibility (like that of Jupiter) in terms of its dynamics. In this paper we expand on previous work and present a new model of Saturn's magnetopause. Using a Newtonian form of the pressure balance equation, we estimate the solar wind dynamic pressure at each magnetopause crossing by the Cassini spacecraft between Saturn Orbit Insertion in June 2004 and January 2006. We build on previous findings by including an improved estimate for the solar wind thermal pressure and include low-energy particle pressures from the Cassini plasma spectrometer's electron spectrometer and high-energy particle pressures from the Cassini magnetospheric imaging instrument. Our improved model has a size-pressure dependence described by a power law $D_P^{-1/5.0 \pm 0.8}$. This exponent is consistent with that derived from numerical magnetohydrodynamic simulations.

Citation: Kanani, S. J., et al. (2010), A new form of Saturn's magnetopause using a dynamic pressure balance model, based on in situ, multi-instrument Cassini measurements, *J. Geophys. Res.*, *115*, A06207, doi:10.1029/2009JA014262.

1. Introduction

1.1. The Magnetopause

[2] The magnetopause is a magnetic and plasma boundary formed between a magnetized planet's magnetic field and the shocked solar wind, separating the solar wind plasma from the planetary plasma. Saturn's magnetopause was detected for the first time in 1979 by Pioneer 11, then by Voyager 1 in 1980 and Voyager 2 in 1981 [*Russell and Luhmann*, 1997].

[3] Saturn has many sources of plasma, including its rings, the solar wind, the ionosphere, and its moons. The Cassini spacecraft has confirmed that the plasma environment is mainly composed of water-based molecular and atomic ions [*Young et al.*, 2004]. Three fundamentally different regions of plasma have been identified: the hot outer magnetosphere, the extended plasma sheet, and the inner plasma torus. The hot outer region of the magnetosphere is where suprathermal electrons dominate the electron pressure and density, whereas the plasma sheet and torus have enhanced levels of cold plasma relative to the outer magnetosphere [*Sittler et al.*, 1983]. In contrast to the terrestrial magnetosphere, these internal magnetospheric plasma sources introduce significant amounts of plasma into the system, which, when heated, contributes an important hot plasma pressure component that plays an important role in determining the configuration of the magnetosphere and hence magnetopause. Periodic modulations of internal plasma pressures can lead to periodic modulations of the magnetopause boundary layer [*Clarke et al.*, 2006].

[4] The solar wind and interplanetary magnetic field (IMF) characteristics at ~9 AU are somewhat different from those at Earth. Proton number densities were measured by Cassini to be in the range of 0.002 to 0.4 cm^{-3} and flow velocities range between 400 and 600 km s^{-1} [*Crary et al.*, 2005]. The main component of pressure in the solar wind is the dynamic pressure, $D_P = \rho u_{SW}^2$, where ρ is the solar wind mass density and u_{SW} is the solar wind velocity. The solar wind is dominantly composed of protons but also includes between ~4% and 20% doubly ionized helium [*Aellig et al.*, 2001].

[1]Mullard Space Science Laboratory, University College London, London, UK.
[2]Also at The Centre for Planetary Sciences at University College London/Birkbeck, London, UK.
[3]Los Alamos National Laboratory, Los Alamos, New Mexico, USA.
[4]Academy of Athens, Athens, Greece.
[5]Applied Physics Laboratory, Johns Hopkins University, Baltimore, Maryland, USA.
[6]Imperial College London, London, UK.
[7]Southwest Research Institute, San Antonio, Texas, USA.
[8]University of Michigan, Ann Arbor, Michigan, USA.
[9]Max-Planck-Institut für Sonnensystemforschung, Katlenberg-Lindau, Germany.

0148-0227/10/2009JA014262

1.2. The Pressure Balance Equation

[5] The magnetopause can be considered as a surface where the total (particle and field) pressure inside the magnetosphere balances the total pressure in the magnetosheath. In reality these pressures will not be perfectly balanced and the magnetopause will be in constant motion. Increases in solar wind dynamic pressure cause the magnetopause to contract, the magnetosphere to compress, and the magnetic field strength to increase, which, as a consequence, results in a magnetosphere exerting a greater outward pressure on the magnetosheath and reaching a new equilibrium magnetopause location. However, to first order, one can consider the magnetopause to be a pressure-balance surface, and as a simple approximation of this equilibrium, the magnetic pressure inside the magnetosphere balances the dynamic pressure of the solar wind ($D_p = \rho u_{\mathrm{SW}}^2$):

$$\rho u_{\mathrm{SW}}^2 = \frac{B^2}{2\mu_0}, \tag{1}$$

where B is the magnetic field intensity inside the magnetosphere and μ_0 is the permeability of free space. Knowing B as a function of distance from the planet allows one to construct an expression for the standoff distance, R_0, of the magnetopause as a function of the dynamic pressure. For a pure dipole, $B \sim r^{-3}$, where r is the distance on the dipole equator, hence $D_p \sim r^{-6}$ and the standoff distance can be written $R_0 \sim D_P^{-1/6}$. This relationship has been confirmed by modeling of the terrestrial magnetopause [e.g., *Shue et al.*, 1997]. However, some magnetospheric fields may not be correctly modeled as a dipole with a fixed dipole moment, favoring instead a stretched configuration with a magnetic field strength that varies more slowly than R_0^{-3}, which requires a smaller increase in D_P to compress the magnetosphere than is required at Earth, and hence the $R_0 \sim D_P^{-1/6}$ power law has a somewhat larger exponent. In general we consider the following expression, where $\alpha = 6$ for a dipole and is smaller for more stretched configurations, and hence α can be considered a diagnostic of stress balance and internal structure within the magnetosphere:

$$R_0 \propto D_p^{-(1/\alpha)}, \tag{2}$$

[6] The pressure balance expression (1) ignores thermal pressure in the magnetosheath and magnetosphere. Equation (3) represents pressure balance including these additional pressures:

$$\rho u^2 + P_0 = \frac{B^2}{2\mu_0} + P_{\mathrm{MS}}. \tag{3}$$

This equation represents the balance between the pressure components of the solar wind plasma, that is, the dynamic pressure and thermal static pressure (P_0), and the pressure components inside the magnetosphere, namely, the magnetic pressure and the internal particle pressures (P_{MS}).

[7] The pressures external to the magnetosphere are actually pressures in the magnetosheath, and to relate them to upstream (solar wind) conditions we can use Bernoulli's equation. Assuming an adiabatic flow between the upstream bow shock and the magnetopause stagnation point, the stagnation pressure can be related to the pressure at any point upstream along the same streamline [*Walker and Russell*, 1995].

$$\frac{p_S}{p} = \left(1 + \frac{\gamma - 1}{2} M_S^2\right)^{\gamma/(\gamma-1)}, \tag{4}$$

where P_S is the stagnation pressure, P is the pressure at a point along the streamline, γ is the ratio of specific heats, and M_S is the sonic Mach number ($M_S = u(\rho/\gamma \mathrm{p})^{0.5}$). Using the Rankine-Hugoniot jump conditions, where the subscript SW refers to the solar wind, and combining these with the stagnation pressure equation, we obtain the equation relating the stagnation pressure to the solar wind thermal pressure:

$$P_S = p_{\mathrm{SW}} \left(\frac{(\gamma+1)^{\gamma+1} \left(\frac{M_{\mathrm{SW}}^2}{2}\right)}{2\gamma M_{\mathrm{SW}}^2 - (\gamma - 1)} \right)^{[(\gamma-1)-1]}, \tag{5}$$

$$P_S = k \rho_{\mathrm{SW}} u_{\mathrm{SW}}^2, \tag{6}$$

where

$$k = \frac{p_S}{\rho_{\mathrm{SW}} u_{\mathrm{SW}}^2} = \left(\frac{\gamma+1}{2}\right)^{(\gamma+1)/(\gamma-1)} \cdot \frac{1}{\gamma \left[\gamma - (\gamma-1)/2M_{\mathrm{SW}}^2\right]^{1/(\gamma-1)}}. \tag{7}$$

The coefficient k indicates by how much the pressure is diminished by the divergence of the flow and relates the dynamic pressure to the thermal pressure for the solar wind. For $\gamma = 5/3$ and $M_{\mathrm{SW}} = \infty$, $k = 0.881$, which is a reasonable assumption for Saturn, where the solar wind is a high Mach number regime. It is thus necessary to include k in the pressure balance equation as it relates the dynamic pressure in the solar wind to that in the magnetosheath.

[8] Away from the stagnation point these pressures are modified by flaring of the magnetopause, such that the plasma is no longer normally incident on the magnetopause. The flaring angle Ψ is the angle between the solar wind direction and the local normal to the magnetopause and is 0° for normal incidence (at the stagnation point). The flaring angle can be found from the cross product of the normal vector and the solar wind direction. The equation below is based on equation (3) but includes the k factor and terms to account for the flaring angle, so is valid everywhere on the magnetopause, not just at the stagnation point.

$$k D_p \cos^2 \Psi + P_0 = \frac{B^2}{2\mu_0} + P_{\mathrm{MS}}. \tag{8}$$

At the subsolar point $\cos^2 \Psi$ is close to unity and the dynamic pressure dominates in this pressure balance, but as $\cos^2 \Psi$ decreases downstream the thermal pressure dominates. *Petrinec and Russell* [1997] showed that using equation (8) and applying Bernoulli's equation along a streamline adjacent to the magnetopause resulted in imaginary flow velocities in the subsolar region. Hence, a $\sin^2 \Psi$ term is applied to the solar wind thermal pressure term in equation (8) to force the flow velocity to be real in the

subsolar region. The equation without the $\sin^2\Psi$ provides reasonably accurate results for high Mach number regimes, but including the term is the simplest formulation of the equation that satisfies both the demands of hydrodynamic flow at the stagnation point and the pressure balance demands downtail [*Petrinec and Russell*, 1997], as shown in the following equation:

$$kD_P \cos^2\Psi + P_0 \sin^2\Psi = \frac{B^2}{2\mu_0} + P_{\mathrm{MS}}, \tag{9}$$

[9] Studies of the terrestrial magnetopause are able to use monitors of the upstream solar wind conditions and hence the position of the magnetopause, as determined by particle and field data from a spacecraft, can be directly related to the upstream solar wind conditions. For the outer planets there is no upstream monitor, hence a pressure balance method is used in which equation (9) is applied to the measured interior magnetospheric pressures, allowing for an estimation of the dynamic pressure at each crossing of the magnetopause.

[10] *Arridge et al.* [2006] used this pressure balance technique to develop a new model for Saturn's magnetopause but did not explicitly include the effects of internal particle pressure inside the magnetosphere. This paper addresses the closing comments of *Arridge et al.* [2006], who realized that their model required further attention to account for the effect of internal plasma pressure on the pressure balance and the assumption of a constant static pressure. Energetic particle pressures are now available and we can incorporate the internal pressures in Saturn's magnetosphere into the pressure balance equation. We can also investigate the static pressure influences and thus establish an improved model.

2. Previous Models

[11] There are many models that estimate the location of a planetary magnetopause, making investigation of its behavior possible [e.g., *Sibeck et al.*, 1991; *Kawano et al.*, 1999; *Joy et al.*, 2002; *Hendricks et al.*, 2005]. It has been demonstrated that the power law relationship for a dipole magnetic field with a fixed magnetic moment [e.g., *Shue et al.*, 1997], is valid at Earth's magnetopause, as the plasma does not contribute much to the total pressure near the magnetopause and the ring current does not change significantly with system size [e.g., *Bunce et al.*, 2007]. For Jupiter the pressure balance method yields an exponent between −1/4 and −1/5 [e.g., *Slavin et al.*, 1985; *Huddleston et al.*, 1998], and for Saturn different studies have shown both a terrestrial-type −1/6 [e.g., *Slavin et al.*, 1985] and a jovian-like −1/4 [*Arridge et al.*, 2006] response.

[12] Three types of pressure balance models of Saturn's magnetopause have been developed: those by *Slavin et al.* [1983, 1985], *Maurice et al.* [1996] and *Arridge et al.* [2006]. The *Slavin et al.* [1985] model, herein referred to as S85, used the pressure balance equation expressed in equation (8) to derive a relationship between the standoff distance and the dynamic pressure. S85 assumed $k = 1$ and model did not include internal plasma pressures so the P_{MS} term in equation (8) was not used. S85 used the pressure balance method to infer D_P and fitted a conic section to a limited set of magnetopause crossings identified in Pioneer 11 and Voyager 1 and 2 data. S85 found $\alpha = 6.1$, that is, a magnetopause that scaled as a terrestrial magnetopause, but with increased flaring. However, the model was valid only between the subsolar point and the same distance tailward, between 19 and −19 R_S (Saturn radii). They argued that the increased flaring was due to the ratio between the solar wind dynamic and thermal pressures. *Maurice et al.* [1996] used a model for Saturn's magnetospheric magnetic field to develop a new model for Saturn's magnetopause. They used the field model to calculate the magnetic field pressure inside the magnetosphere and a numerical technique to find the surface that was in pressure balance with the solar wind (via equation (1)). Their model magnetopause was considerably less flared compared to the S85 model.

[13] *Hansen et al.* [2005], herein referred to as H05, used the results of MHD simulations to investigate how the distance to the subsolar magnetopause varied with dynamic pressure. The model included internal plasma sources but the internal mass loading rate was adjusted so that the magnetopause was located where Cassini actually crossed the magnetopause on its approach and insertion orbit. The model implicitly includes the effects of internal plasma pressure but does not include the multiple plasma populations that are present in Saturn's magnetosphere or the high energy density in some of the energetic populations. H05 found that the magnetopause is less flared than in previous models and is asymmetrical in the dawn-dusk meridian. The modeled magnetotail showed a hinge at 20 R_S due to the inclination of Saturn's dipole to the solar wind, similar to that identified in Cassini observations [*Arridge et al.*, 2008a; *Carbary et al.*, 2008]. To establish a power law relationship between R_0 and D_P, H05 used a constant solar wind speed and varied D_P by controlling the solar wind plasma density. H05 found an α value of 5.2, between values previously calculated for Earth and Jupiter; corresponding to a magnetopause that is neither as rigid as the Earth's nor as compressible as Jupiter's.

[14] Using the lack of upstream solar wind dynamic pressure measurements as a prompt, the authors of the *Arridge et al.* [2006] study (herein referred to as A06) presented a new technique for making a pressure-dependent model. The model used data from Cassini and Voyagers 1 and 2 and the more elaborate form of the pressure balance equation as expressed in equation (9). For A06, $k = 0.881$, which is valid in high Mach number regimes, as discussed in section 1.

[15] The A06 model magnetopause is rotationally symmetric about the x axis, and the polar coordinates of the magnetopause crossings can be calculated using equation (10). R is the distance from the planet to a point on the magnetopause and θ is the angle subtended at the planet by the x axis and a position vector to a point on the magnetopause:

$$R = R_0 \left(\frac{2}{1 + \cos\theta} \right)^K. \tag{10}$$

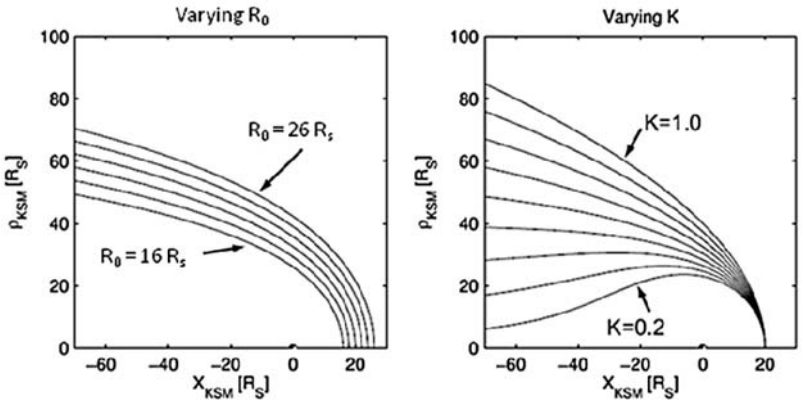

Figure 1. The geometry of the *Arridge et al.* [2006] (A06) magnetopause model, demonstrating the effects of the varying standoff distance R_0 (left) and K (right) on the size and shape of the magnetopause, where $K = 0.7$ (left) and $R_0 = 20\ R_S$ (right). [Taken from *Arridge*, 2007.]

[16] The pressure-dependent size and shape of the magnetopause are set through equations (11) and (12), respectively.

$$R_0 = a_1 D_P^{-a_2}. \tag{11}$$

$$K = a_3 + a_4 D_P. \tag{12}$$

[17] Figure 1 demonstrates how varying R_0 and K values affect the shape of the model magnetopause. R_0 affects the size, and varying K changes how much the magnetopause flares. The dynamic pressure is used to create a model magnetopause, by fitting for modeled polar coordinates. The process uses equations (10)–(12). Dynamic pressures are inferred by iteratively fitting the magnetopause shape for coefficients a_i. The process is presented as a flowchart in Figure 2. At each iteration, Ψ and D_P are estimated, then the root mean square (RMS) residual is found between the observed and the modeled R values, and once the tolerance of this RMS deviation is reached, the fitting is complete. In fitting for the coefficients the model will converge successfully for any inputted values. The algorithm employed is the nonlinear fitting Levenberg-Marquadt routine, which searches for a_i by minimizing the RMS residual. The process converges so that estimated D_P values are consistent with fitted model parameters.

[18] A06 obtain Ψ directly from model normals; the model normal vector is calculated at each iteration, and Ψ is computed from the scalar product of the model normal with the solar wind direction. This means that Ψ is model dependent; assuming a pressure balance, the magnetopause geometry affects the dynamic pressure. At each iteration D_P is also estimated as the coefficients a_i are evaluated; thus, as the shape of the model changes, D_P and the flaring angle also change for current a_i values.

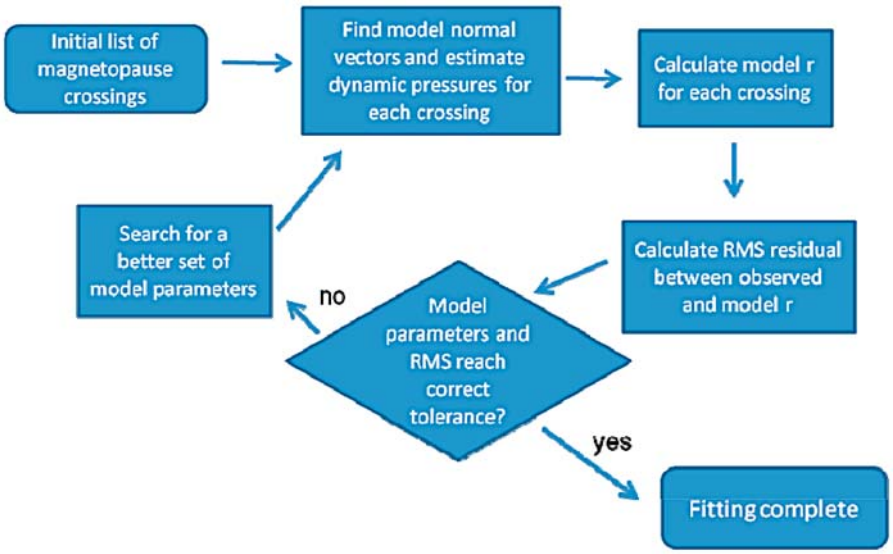

Figure 2. Flow diagram explaining the algorithm for fitting the new model magnetopause, as discussed in section 2.

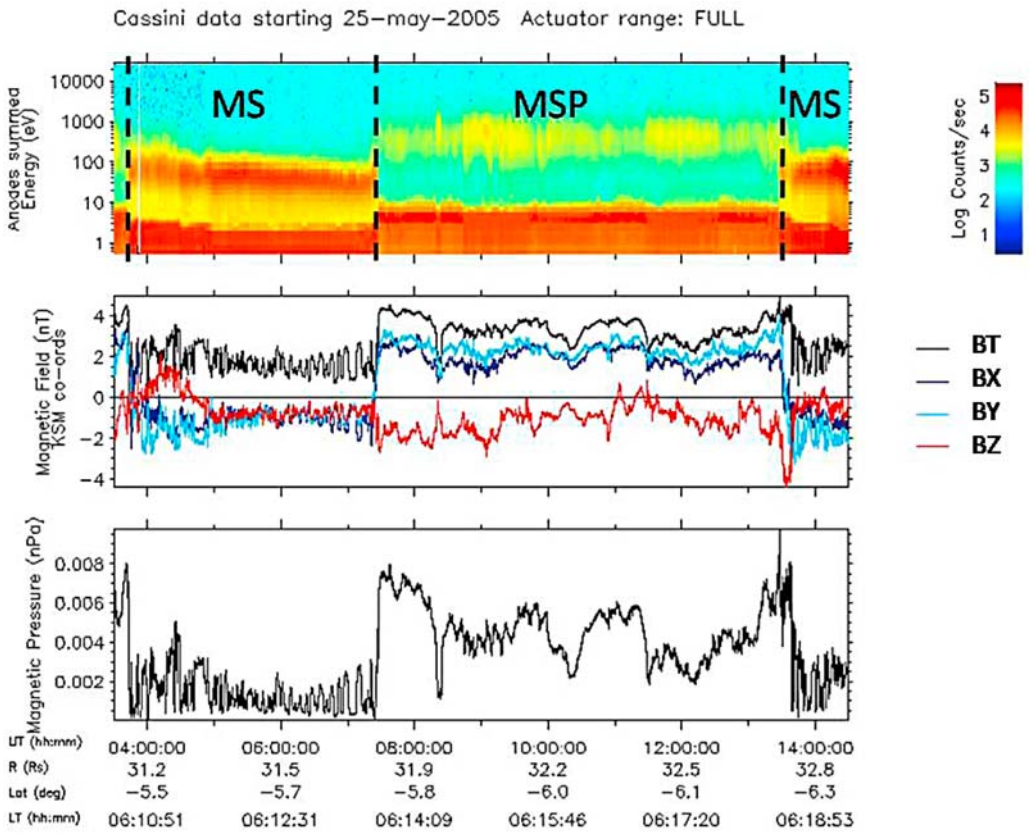

Figure 3. Observations at the magnetopause obtained by Cassini electron spectrometer (CAPS-ELS) and MAG. (top) Energy-time spectrogram in units of electron count rate; (middle) magnetic field in Kronocentric Solar Magnetospheric (KSM) coordinates; (bottom) magnetic pressure from MAG data. MS, magnetosheath; MSP, magnetosphere. A clear-cut set of magnetopause crossings is presented, located at approximately 0350 UT (outbound), 0730 UT (inbound), and 1340 UT (outbound). It is easy to see the crossings in all data sets.

[19] The A06 model has a pressure response described by $\alpha = 4.3 \pm 0.4$, which represents a magnetosphere that is as compressible as the Jovian system. However, the model does not take polar flattening into account owing to its axisymmetry, which was forced on the model because of the lack of high-latitude crossings, a problem that also presents itself in the new model.

[20] A06 estimated the effects of a high plasma β on the model magnetopause by doubling the magnetic pressures at equatorial locations and inferring a power law relationship from this. In a high β regime, such as that discovered in the kronian magnetosphere [*Sergis et al.*, 2007], A06 found a modeled power law of $\alpha = 5.5 \pm 0.7$.

3. Method

3.1. The New Model

[21] The new model uses the A06 numerical algorithm for calculating Ψ and D_P, as discussed in section 2. Changes were made to the A06 form of the pressure balance equation to address the issues highlighted previously. A constant static pressure (P_0) value was replaced with a static pressure, dependent on the dynamic pressure. When the results of the A06 pressure balance equation were compared to numerical MHD simulations by H05, it became apparent that the static solar wind pressure component was too small in A06. Larger P_0 values failed to correct this, producing inconsistent results and often negative dynamic pressures. It was recognized that P_0 was varying with solar wind density, and so our model employs a solar wind density-dependent static pressure component. At constant temperature, the solar wind static pressure varies with density via $P_0 = nK_BT$, where n is the number density, T is the temperature, and k_B is Boltzmann's constant. Since the pressure balance equation is dependent on the dynamic pressure, we expressed density, and thus P_0, as a function of dynamic pressure assuming a fixed solar wind speed and helium abundance. A factor of 1.16 was introduced to take into account an approximate 4% contribution of He^{2+} in the solar wind with a temperature equal to approximately four times the temperature of protons [*Slavin et al.*, 1985]. Varying this factor did not have any significant effect on the fitted model parameters. The validity of assuming a fixed solar wind velocity was also tested by varying the velocity between 400 and 600 km/s. It was found that different values of u_{SW} did not notably change the best-fit coefficients beyond their uncertainties.

[22] The most significant modification to the A06 methodology was to include internal plasma pressures in the pressure balance equation to investigate the effects of high plasma β regimes. Averages of high-energy ion pressures

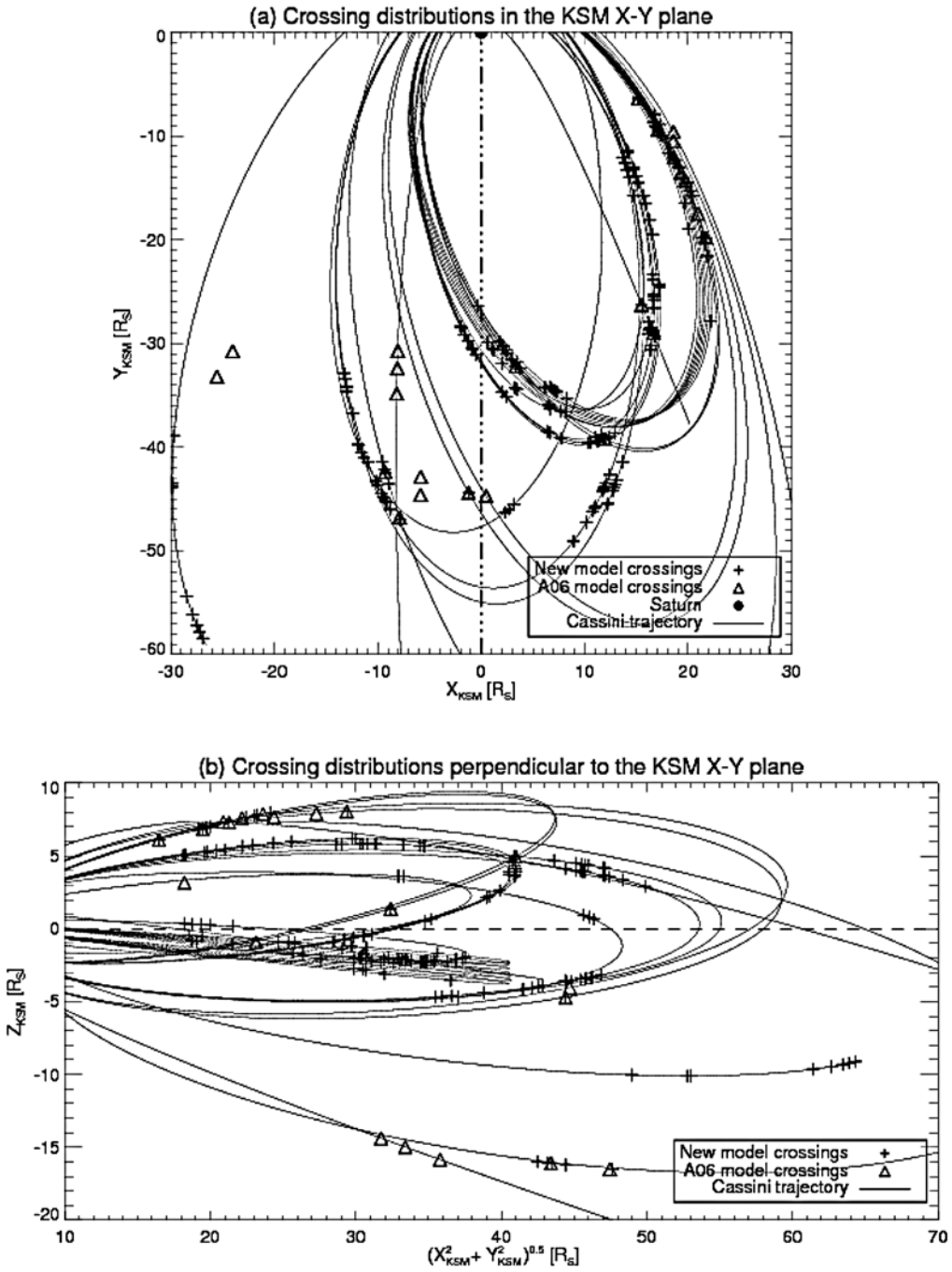

Figure 4. Magnetopause crossings used in this study. (a) All the crossings in the KSM plane. The plot shows that most crossings are in the noon-dawn local time sector. Triangles show crossings used in the A06 model. Crosses denote crossings used in the new model. The filled circle is a representation of Saturn's position and the Sun is to the right. (b) A representation of the crossings in cylindrical coordinates to show the low-latitude coverage. Cassini's trajectory for the period is shown by the solid line.

were taken from the magnetospheric imaging instrument (MIMI) for 5 min intervals just inside the magnetopause at each crossing location [*Sergis et al.*, 2009]. Corresponding averages of low-energy electron pressures were taken from the Cassini electron spectrometer (CAPS-ELS).

[23] Low-energy proton pressures were estimated using 20% of the low-energy electron pressures given the assumption that the total ion number density is ~20% protons. The proton temperature is approximately the same as the electron temperature. This assumption is based on the best available data at present; note that a possible contribution from water-group ions has not been included in the CAPS energy range owing to the fact that the water-group pressure is included in the energetic pressure calculation.

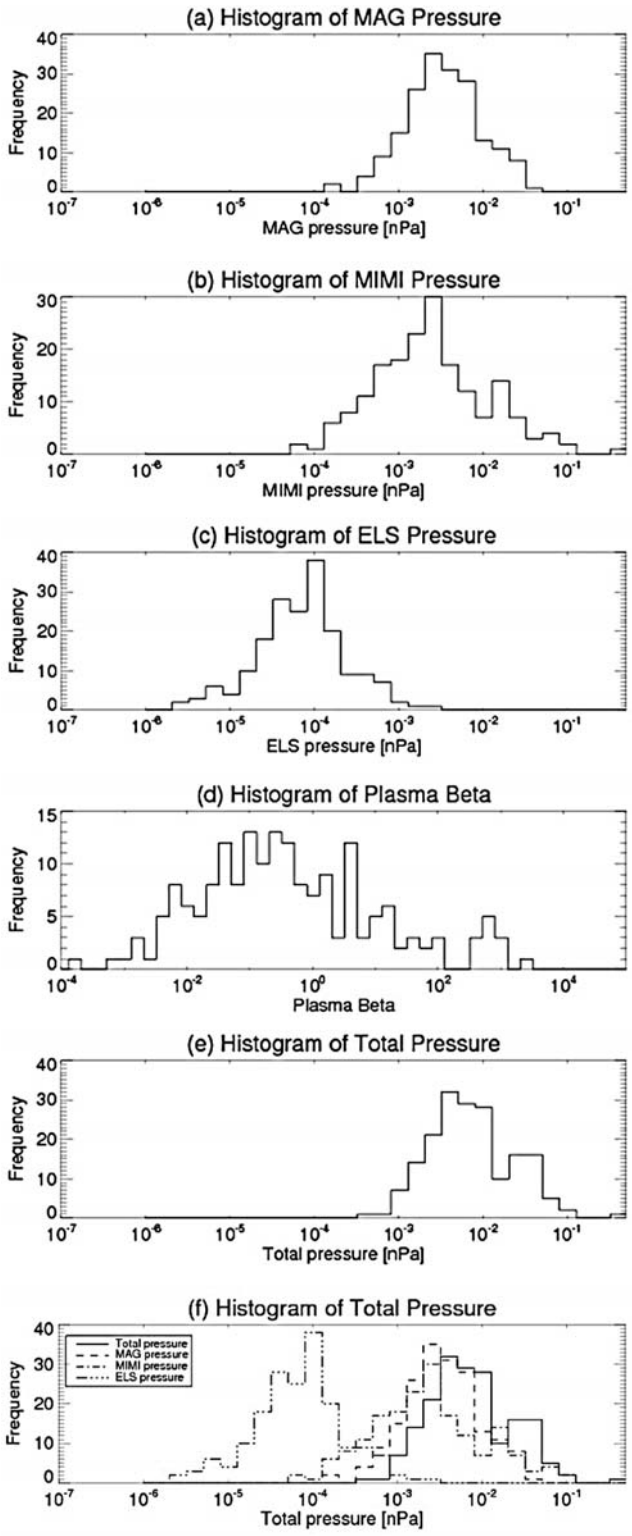

Figure 5. Histograms of pressure and plasma parameter distributions: (a) magnetic pressure from the MAG instrument; (b) high-energy particle pressure from the magnetospheric imaging instrument (MIMI); (c) low-energy electron pressure from the CAPS-ELS instrument; (d) plasma β; (e, f) histograms showing the total pressure contributions inside the magnetosphere (with and without individual components overlain, respectively).

This cannot be improved at this time without a full multispecies pressure calculation from eV to keV ranges that account for the ion bulk velocity. Including these projected proton pressures generate results within the error margins, so the final results are stated without these estimates. The final pressure balance equation is expressed in equation (13), where m_p is the proton mass. Knowing the magnetic pressure, the MIMI pressure, and the CAPS-ELS pressure, and inferring Ψ from the model normals makes it possible to calculate D_P from the pressure balance equation.

$$kD_P \cos^2\Psi + \frac{k_B T_{\mathrm{SW}}}{1.16 m_p u_{\mathrm{SW}}^2} D_P \sin^2\Psi = \frac{B^2}{2\mu_0} + P_{\mathrm{MIMI}} + P_{\mathrm{ELS}}. \quad (13)$$

3.2. The Data

[24] The coordinate system used for the new model is the Kronocentric Solar Magnetospheric (KSM) system, which is Saturn centered, where the x axis points toward the Sun, the x-z plane contains Saturn's centered magnetic dipole moment, and the y axis completes the right-hand set, pointing duskward.

[25] The magnetopause crossings used in this study were identified using 1 s averaged CAPS-ELS data covering the period from before Saturn Orbit Insertion in June 2004 until the end of January 2006. In ELS data a magnetopause crossing can be identified as a boundary between higher-density, lower-temperature electrons in the magnetosheath and lower-density, higher-temperature electrons in the magnetosphere. A rotation in the magnetic field to a southward orientation is also seen as the boundary is crossed. However, variations in the plasma data that are not apparent in the magnetic field data can also be identified as crossings, as these are usually associated with the entry of the spacecraft into a boundary layer. Often, the crossings involved a high magnetic shear and were very apparent in all data sets. In some cases the crossing locations were not so clear in the magnetometer data; when this was the case, the plasma data were taken to be more reliable than the magnetic field data for the purpose of placing crossing locations. Figure 3 illustrates three typical clear magnetopause crossings, two into the magnetosheath and one into the magnetosphere, from 25 May 2005 when Cassini was slightly below the equatorial plane, at ~32 R_S from Saturn on the dawn flank. Each crossing of the magnetopause is associated with a large rotation in the magnetic field and an increase in the field strength. High-frequency waves and mirror-mode-type structures are visible in the magnetosheath. In the plasma data, upstream of the magnetopause the colder, denser magnetosheath electron population is apparent, whereas downstream of the boundary more energetic magnetospheric electrons are evident. Intense counts of electrons below about 10 eV are trapped spacecraft photoelectrons.

[26] The temporal uncertainty in locating magnetopause crossings is not more than 10 min, which corresponds to about 0.1 R_S. This is well within the RMS spread for the model. The data collection consists of a set of 191 crossings [*McAndrews*, 2007] that were spatially averaged to remove any bias due to boundary waves, rapid boundary motion, and the spacecraft trajectory. Spatially averaging crossings

Table 1. Values for the Model Coefficients and Root Mean Square (RMS) for the A06 and New Models Calculated Using Equations (11) and (12), Showing the Differences Between α and the RMS Values for the Two Models

Parameter	A06 model	New model
a_1	9.7 ± 1.0	10.3 ± 1.7
a_2	0.24 ± 0.02	0.20 ± 0.03
a_3	0.77 ± 0.03	0.73 ± 0.07
a_4	−1.5 ± 0.3	0.4 ± 0.5
α value	4.3±0.4	5.0 ± 0.8
RMS	1.238	3.603
	3.82 (new model)[a]	
No. of data points used (No. spatially averaged)	64 (26)	191 (68)

[a]Using new model crossings and A06 model coefficients, the associated RMS was found to be 3.82, higher than the RMS for the new model.

within 1 R_S of each other reduced the data set to 68 crossings. Figure 4 shows the spatial distribution of the magnetopause crossings used in A06 and the new study. Figure 4a demonstrates that the crossings are distributed evenly between local noon and the dawn flank/postmidnight sector at low latitudes. Figure 4b illustrates the distribution about the KSM x-y plane and shows the predominance of the crossings about the equator. The lack of high-latitude crossings may affect the outcome of the new study; this is discussed in further detail in section 4.

[27] Figure 5 shows the histograms of the distribution of the magnetospheric pressure inside the magnetopause for the crossings used in this study. The inclusion for the first time of all internal pressures provides an excellent insight into the effects of the contributions of different partial pressures adjacent to the magnetopause inside the kronian magnetosphere. Figure 5a shows a histogram of the magnetic pressures inside the magnetosphere, taken from the MAG instrument. The magnetic pressure varies from 10^{-4} to $<10^{-1}$ nPa (corresponding to field strengths between 0.5 and 15 nT), with a peak near 3×10^{-3} nPa. This corresponds to a field strength of several nanoteslas, which is common in Saturn's outer magnetosphere [e.g., *Arridge et al.*, 2008b]. Figure 5b illustrates the distribution of suprathermal particle pressures inside the magnetopause, taken from the MIMI instrument. Here pressures vary between 10^{-4} and 1 nPa, with a peak at approximately 3×10^{-3} nPa, similar to the magnetic pressure. Figure 5c shows low-energy electron pressures inside the magnetosphere, from the ELS instrument. The pressures due to low-energy particles are an order of magnitude less than the magnetic and suprathermal ion pressure, with a peak pressure of approximately 10^{-4} nPa, but the distribution has a width of about four orders of magnitude, which is similar to the magnetic and suprathermal ion pressure. The total pressure histograms, Figures 5e and 5f, are thus dominated by the distribution of the suprathermal ion and magnetic pressure as the electron pressure is so low. These histograms also show possible evidence of the bimodal distribution as discussed by *Achilleos et al.* [2008], although these effects are beyond the scope of this model. Finally, Figure 5d shows plasma β inside the magnetopause that is found to range between 10^{-4} and 10^{3} and has a peak near 0.4, although the peak is quite broad, extending between ~0.03 and 1.0. This highlights the clear importance of the plasma pressure for a large proportion of the magnetopause crossings in this study, but not all.

4. Discussion

[28] Table 1 shows the values for the coefficients and RMS for A06 and our new model. The A06 and new models are also compared in Figure 6. First, the size coefficient a_1 is slightly larger than A06 but is in agreement with A06 within the estimated uncertainty. To first order the introduction of additional sources of pressure inside the magnetosphere results in the estimated dynamic pressure being somewhat larger at each crossing. Hence, the model magnetopause will be slightly larger for the same dynamic pressure compared to A06.

[29] The flaring parameter a_3 is slightly smaller in the new model compared to A06, resulting in a slightly more streamlined shape. We attribute this to the direct inclusion of a dynamic pressure-dependent P_0 in the new model, which increases the static pressure on the flanks and streamlining the obstacle. The pressure-dependent flaring parameter a_4 has changed the most between A06 and the new model; the large relative uncertainty in this parameter perhaps suggests that this parameter cannot be accurately resolved by the fitting technique and/or data set used.

[30] The power law dependence of the dynamic pressure on the size of the magnetosphere is also consistent with A06 within the estimated uncertainties. The power law $R_0 \sim D_p^{-1/\alpha}$ is described by $\alpha = 5.0 \pm 0.8$, compared to 6.1 for S85 and 4.3 ± 0.4 for A06. A power law exponent with $\alpha < 6$ indicates a magnetosphere that does not scale as a dipole with a fixed moment but is more compressible, possibly giving evidence for the disc-like geometry that is thought to exist at Saturn [*Arridge et al.*, 2008b], enhanced plasma pressure within the disc, and response of the centrifugal component of the ring current to changes in system size [*Bunce et al.*, 2007]. Thus, while the inclusion of magnetospheric plasma pressure has modified the value of α, the new value is still consistent with A06 and with the idea of a significantly compressible magnetosphere. This is in agreement with the results from MHD models presented by H05 but does not support the Pioneer/Voyager-era modeling in S85.

Figure 6. The new model magnetopause shape. (a) The new model magnetopause (dotted line) with crosses denoting the new model, scaled crossings, and the A06 model magnetopause (dashed line) with triangles denoting the A06 model, scaled crossings, both scaled to a standoff distance of 20 R_S. This gives a D_P of 0.036 and 0.043 nPa for the new model and A06, respectively. It can be seen that the new model is less flared. (b) The new magnetopause shape scaled so that the standoff distance is at 21 and 27 R_S, giving D_P as 0.028 and 0.008 nPa, respectively. Crossings are, once again, scaled for relevant dynamic pressures. In each of these plots the coordinates are along the X_{KSM} axis and in the direction perpendicular to this, $(Y_{\mathrm{KSM}}^2 + Z_{\mathrm{KSM}}^2)^{1/2}$.

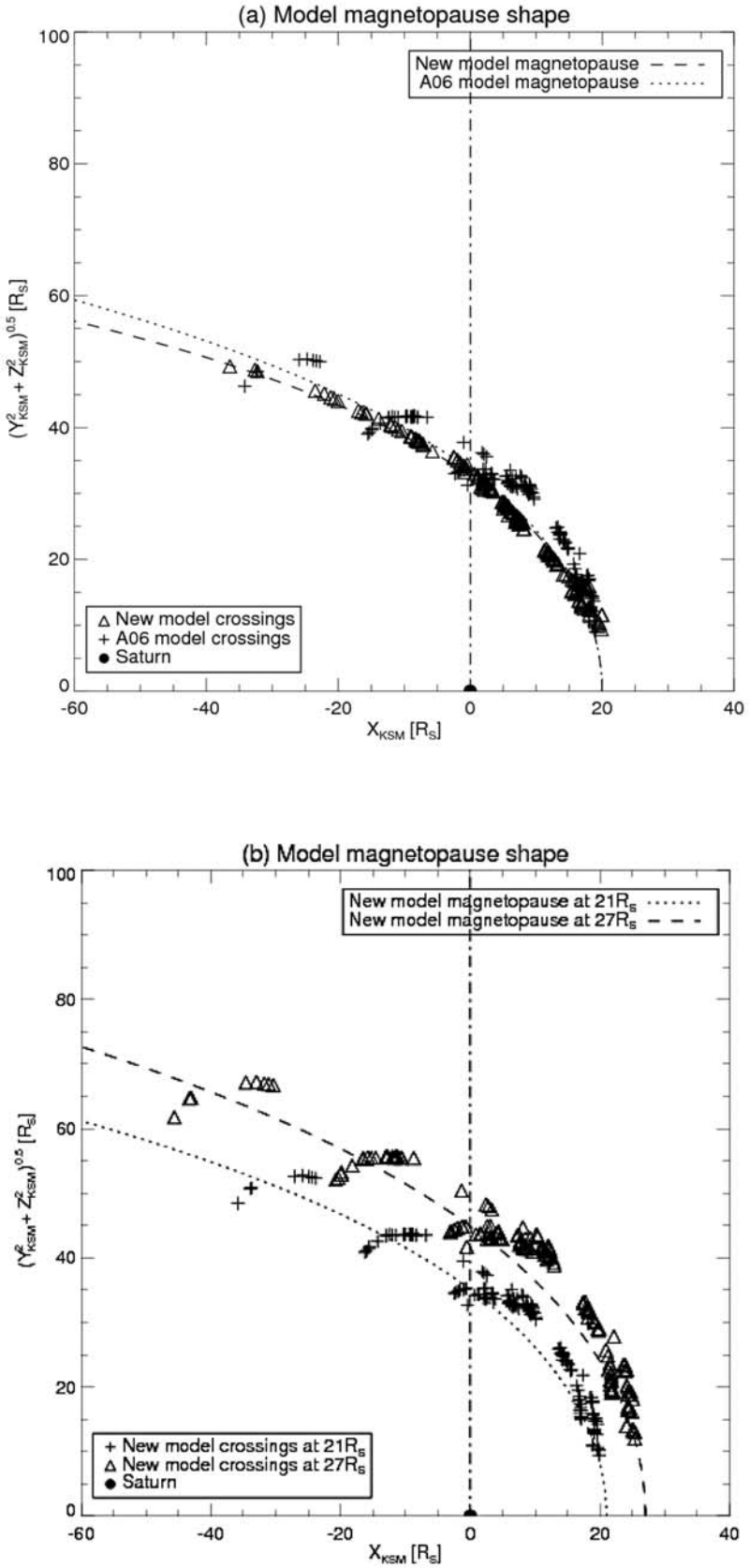
(a) Model magnetopause shape
New model magnetopause
A06 model magnetopause
New model crossings
A06 model crossings
Saturn
$(Y_{KSM}^2 + Z_{KSM}^2)^{0.5}$ [R_S]
X_{KSM} [R_S]
(b) Model magnetopause shape
New model magnetopause at 21R_S
New model magnetopause at 27R_S
New model crossings at 21R_S
New model crossings at 27R_S
Saturn
$(Y_{KSM}^2 + Z_{KSM}^2)^{0.5}$ [R_S]
X_{KSM} [R_S]

Figure 6

[31] Figure 6 illustrates the new model magnetopause shape, compared with A06 (Figure 6a) and for two dynamic pressures (Figure 6b), with crossings scaled for relevant dynamic pressures. The difference in the geometry of the new model with A06 is clear from Figure 6a. Figure 6b shows the geometry of the new model, with magnetopause locations scaled to represent high- and low-pressure solar wind conditions. The crossings are spread about the model, showing the validity of the assumptions used in the fitting. However, the crossings for this model are constrained to mainly dayside and lower latitudes, so this will have a bias on the results. In particular, we were not able to identify a dawn-dusk or north-south asymmetry owing to the axisymmetry of the model and the spacecraft coverage of the magnetosphere.

[32] Variations between the models are due to the expanded data set and the inclusion of variable solar wind thermal pressure and magnetospheric plasma pressure effects. The results of this analysis show that the assumption of a vacuum magnetosphere is not entirely unreasonable for the data used by A06. The model derived in our study is close to that derived by A06 in their "high-β correction," although smaller, and so this also supports the idea that the A06 high-β correction was overcorrecting to some degree. Finally, the RMS value is higher for the new model than for A06, but this might be expected, owing to the increased number of input parameters. The new model was run using the best-fit coefficient values for the A06 model and the associated RMS was found to be 3.82. This shows that while the two models are similar, including actual magnetospheric plasma data in the new model gives improved results. We have not included effects relating to periodic motion of the magnetopause [e.g., *Clarke et al.*, 2006] but note that the peak-to-trough amplitude for such oscillations is about 2 R_S, which is smaller than the RMS of our new model. Hence, such oscillations represent noise in the context of this work; these effects are implicitly taken into account within the model. Future work may attempt to investigate whether the magnetopause is more or less compressible during such outward or inward periodic displacements.

[33] Other future work on this model could include using a larger database of crossings, making the model more current. A comparison of the model dynamic pressures with actual measurements would be hugely beneficial in aiding its validity. The crossings used are primarily in the dawn sector at low latitudes, which means that this model cannot account for any polar flattening effect, but evidence for such an effect is being sought (*Achilleos et al.*, private communication). A lack of high-latitude crossings has prevented the investigation of this effect so future attempts to include these in the model would be important for the global understanding of the system.

5. Conclusions

[34] A new model of Saturn's magnetopause was created using a multi-instrument Cassini data analysis. In the absence of an upstream monitor of the solar wind, dynamic pressures were calculated using an iterative process to fit a pressure balance model, including in it a variable solar wind thermal pressure and taking into consideration the total magnetospheric plasma pressure. The results support the finding of A06 and H05 that the magnetopause size scales differ significantly from those expected of a dipole with a fixed magnetic moment. This indicates that cold plasma and important centrifugal forces within the ring current are important in determining the pressure-dependent location of the magnetopause [*Bunce et al.*, 2007]. The inclusion of hot plasma pressure in our new model has not significantly changed this finding, although there is some evidence for a slight change in the overall size of the magnetopause for a given solar wind dynamic pressure.

[35] As a result of including a dynamic pressure-dependent P_0, the new model has a less flared geometry. A sensitivity study was carried out to test the effect of the assumptions that were made regarding the static pressure and it was found that the model was insensitive to variations in solar wind speed and helium abundance. A further sensitivity study was carried out to evaluate the impact of our assumptions regarding the proton pressure inside the magnetosphere, and we found that the model was robust to variations in our assumptions. We have shown that the model has improved on previous models owing to the inclusion of the suprathermal plasma and variable static pressures in the pressure balance equation, providing more realistic results, thus we suggest that it is the most accurate representation of Saturn's magnetopause to date.

[36] **Acknowledgments.** S.J.K. would like to thank the coauthors for useful comments and discussions. S.J.K. would like to thank G. R. Lewis and L. K. Gilbert for their continued work and assistance with ELS data and software. We would like to thank S. Kellock, P. Slootweg, and L. Alconcel at Imperial College London for MAG data processing. Cassini CAPS/ELS and MAG data processing activities are supported in the United Kingdom by STFC. S.J.K. was supported in this work by a STFC Ph.D. Studentship. C.S.A., A.N.F., and A.J.C. were supported by the STFC rolling grant to MSSL/UCL. G.H.J. was supported by an STFC Advanced Fellowship. The work at Los Alamos was performed under the auspices of the U.S. DOE and was supported by the NASA Cassini program.

[37] Zuyin Pu thanks the reviewers for their assistance in evaluating the manuscript.

References

Achilleos, N., et al. (2008), Large-scale dynamics of Saturn's magnetopause: Observations by Cassini, *J. Geophys. Res.*, *113*, A11209, doi:10.1029/2008JA013265.

Aellig, M. R., et al. (2001), The solar wind helium abundance: Variation with wind speed and the solar cycle, *Geophys. Res. Lett.*, *28*(14), 2767–2770, doi:10.1029/2000GL012771.

Arridge, C. S. (2007), On the configuration and dynamics of Saturn's magnetosphere, Ph.D. thesis, Imperial College London.

Arridge, C. S., et al. (2006), Modeling the size and shape of Saturn's magnetopause with variable dynamic pressure, *J. Geophys. Res.*, *111*, A11227, doi:10.1029/2005JA011574.

Arridge, C. S., K. K. Khurana, C. T. Russell, D. J. Southwood, N. Achilleos, M. K. Dougherty, A. J. Coates, and H. K. Leinweber (2008a), Warping of Saturn's magnetospheric and magnetotail current sheets, *J. Geophys. Res.*, *113*, A08217, doi:10.1029/2007JA012963.

Arridge, C. S., C. T. Russell, K. K. Khurana, N. Achilleos, S. W. H. Cowley, M. K. Dougherty, and E. J. Bunce (2008b), Saturn's magnetodisc current sheet, *J. Geophys. Res.*, *113*, A04214, doi:10.1029/2007JA012540.

Bunce, E. J., S. W. H. Cowley, I. I. Alexeev, C. S. Arridge, M. K. Dougherty, J. D. Nichols, and C. T. Russell (2007), Cassini observations of the variation of Saturn's ring current parameters with system size, *J. Geophys. Res.*, *112*, A10202, doi:10.1029/2007JA012275.

Carbary, J. F., D. G. Mitchell, C. Paranicas, E. C. Roelof, and S. M. Krimigis (2008), Direct observation of warping in the plasma sheet of Saturn, L24201, doi:10.1029/2008GL035970.

Clarke, K. E., et al. (2006), Cassini observations of planetary-period oscillations of Saturn's magnetopause, *Geophys. Res. Lett.*, *33*(23), L23104, doi:10.1029/2006GL027821.

Crary, F. J., et al. (2005), Solar wind dynamic pressure and electric field as the main factors controlling Saturn's aurorae, *Nature*, *433*, 720, doi:10.1038/nature03333.

Hansen, K. C., et al. (2005), Global MHD simulations of Saturn's magnetosphere at the time of Cassini approach, *Geophys. Res. Lett.*, *32*, L20S06, doi:10.1029/2005GL022835.

Hendricks, S., et al. (2005), Variability in Saturn's bow shock and magnetopause from Pioneer and Voyager: Probabilistic predictions and initial observations by Cassini, *Geophys. Res. Lett.*, *32*, L20S08, doi:10.1029/2005GL022569.

Huddleston, D. E., et al. (1998), Location and shape of the jovian magnetopause and bow shock, *J. Geophys. Res.*, *103*(E9), 20,075–20,082, doi:10.1029/98JE00394.

Joy, S. P., et al. (2002), Probabilistic models of the Jovian magnetopause and bow shock locations, *J. Geophys. Res.*, *107*(A10), 1309, doi:10.1029/2001JA009146.

Kawano, H., et al. (1999), Magnetopause shape determinations from measured position and estimated flaring angle, *J. Geophys. Res.*, *104*(A1), 247–261, doi:10.1029/98JA02479.

Krimigis, S. M., et al. (2004), Magnetosphere Imaging Instrument (MIMI) on the Cassini mission to Saturn/Titan, *Space Sci. Rev.*, *114*, 233–329, doi:10.1007/s11214-004-1410-8.

Maurice, S., et al. (1996), Geometry of Saturn's magnetopause model, *J. Geophys. Res.*, *101*(A12), 27,053–27,059, doi:10.1029/96JA02605.

McAndrews, H. J. (2007), Cassini observations of low energy electrons in and around Saturn's magnetosphere, Ph.D. thesis, Mullard Space Science Laboratory-Univ. College London.

Petrinec, S. M., and C. T. Russell (1997), Hydrodynamic and MHD equations across the bow shock and along the surfaces of planetary obstacles, *Space Sci. Rev.*, *79*, 757–791, doi:10.1023/A:1004938724300.

Russell, C. T., and J. G. Luhmann (1997), *Encyclopedia of Planetary Sciences*, pp. 718–719, Chapman and Hall, New York.

Sergis, N., et al. (2007), Ring current at Saturn: Energetic particle pressure in Saturn's equatorial magnetosphere measured with Cassini/MIMI, *Geophys. Res. Lett.*, *34*, L09102, doi:10.1029/2006GL029223.

Sergis, N., et al. (2009), Energetic particle pressure in Saturn's magnetosphere measured with the Magnetospheric Imaging Instrument on Cassini, *J. Geophys. Res.*, *114*, A02214, doi:10.1029/2008JA013774.

Shue, J. H., et al. (1997), A new functional form to study the solar wind control of the magnetopause size and shape, *J. Geophys. Res.*, *102*(A5), 9497–9511, doi:10.1029/97JA00196.

Sibeck, D. G., et al. (1991), Solar wind control of the magnetopause shape, location, and motion, *J. Geophys. Res.*, *96*(A4), 5489–5495, doi:10.1029/90JA02464.

Sittler, E. C., et al. (1983), Survey of low-energy plasma electrons in Saturn's magnetosphere, *J. Geophys. Res.*, *88*(A11), 8848–8870, doi:10.1029/JA088iA11p08847.

Slavin, J. A., et al. (1983), A Pioneer-Voyager study of the solar wind interaction with Saturn, *Geophys. Res. Lett.*, *10*(1), 9–12, doi:10.1029/GL010i001p00009.

Slavin, J. A., et al. (1985), Solar wind flow about the outer planets: Gas dynamic modelling of the Jupiter and Saturn bow shocks, *J. Geophys. Res.*, *90*(A7), 6275–6286, doi:10.1029/JA090iA07p06275.

Young, D. T., et al. (2004), Cassini plasma spectrometer investigation, *Space Sci. Rev.*, *114*, 1–112, doi:10.1007/s11214-004-1406-4.

C. S. Arridge, A. J. Coates, A. N. Fazakerley, G. H. Jones, and S. J. Kanani, Mullard Space Science Laboratory, University College London, Holmbury St. Mary, Dorking, Surrey RH5 6NT, UK. (sk2@mssl.ucl.ac.uk)

M. K. Dougherty, Imperial College London, Exhibition Rd. London, SW7 2BZ UK.

K. C. Hansen, University of Michigan, Ann Arbor, MI 48109, USA.

S. M. Krimigis, Applied Physics Laboratory, Johns Hopkins University, Baltimore, MD 21218, USA.

N. Krupp, Max-Planck-Institut für Sonnensystemforschung, Katlenberg-Lindau, Max-Planck-Str. 2, 37191 Germany.

H. J. McAndrews, Los Alamos National Laboratory, Los Alamos, NM 87545, USA.

N. Sergis, Academy of Athens, Soranou Efesiou 4, Papagos, Athens, 10679 Greece.

D. T. Young, Southwest Research Institute, San Antonio, TX 78238, USA.